Published in final edited form as:
*Science*. 2011 November 25; 334(6059): 1097–1103. doi:10.1126/science.1213256.

# A potent and broad neutralizing antibody recognizes and penetrates the HIV glycan shield

**Robert Pejchal**[1,*], **Katie J. Doores**[2,3,*], **Laura M. Walker**[2,*], **Reza Khayat**[1,*], **Po-Ssu Huang**[4,*], **Sheng-Kai Wang**[5], **Robyn L. Stanfield**[1], **Jean-Philippe Julien**[1], **Alejandra Ramos**[2], **Max Crispin**[6], **Rafael Depetris**[7], **Umesh Katpally**[8], **Andre Marozsan**[8], **Albert Cupo**[8], **Sebastien Maloveste**[9], **Yan Liu**[10], **Ryan McBride**[11], **Yukishige Ito**[12], **Rogier W. Sanders**[7,13], **Cassandra Ogohara**[4], **James C. Paulson**[11], **Ten Feizi**[10], **Christopher N. Scanlan**[6], **Chi-Huey Wong**[5], **John P. Moore**[7], **William C. Olson**[8], **Andrew B. Ward**[1], **Pascal Poignard**[2,14], **William R. Schief**[2,4], **Dennis R. Burton**[2,3,†], and **Ian A. Wilson**[1,†]

[1]Department of Molecular Biology, Skaggs Institute for Chemical Biology, and IAVI Neutralizing Antibody Center, The Scripps Research Institute, La Jolla, California 92037, USA [2]Department of Immunology and Microbial Science and IAVI Neutralizing Antibody Center, The Scripps Research Institute, La Jolla, California 92037, USA [3]Ragon Institute of MGH, MIT, and Harvard, Cambridge, Massachusetts 02129, USA [4]Department of Biochemistry, Washington University, Seattle, Washington 98195, USA [5]Department of Chemistry, The Scripps Research Institute, La Jolla, California 92037, USA [6]Oxford Glycobiology Institute, Department of Biochemistry, University of Oxford, South Parks Road, Oxford, OX1 3QU, UK [7]Weill Medical College of Cornell University, New York, NY 10021, USA [8]Progenics Pharmaceuticals, Tarrytown, NY 10591, USA [9]Laboratory of Molecular Microbiology, National Institute of Allergy and Infectious Diseases, National Institutes of Health, Bethesda, MD 20892, USA [10]Glycosciences Laboratory, Department of Medicine, Imperial College London, Hammersmith Campus, Du Cane Road, London, W12 0NN, UK [11]Department of Physiological Chemistry, The Scripps Research Institute, La Jolla, California 92037, USA [12]RIKEN Advanced Science Institute and ERATO JST, 2-1 Hirosawa, Wako, Saitama 351-0198, Japan [13]Department of Medical Microbiology, Academic Medical Center, Amsterdam, The Netherlands [14]International AIDS Vaccine Initiative, New York, New York 10038, USA

## Abstract

The HIV envelope (Env) protein gp120 is protected from antibody recognition by a dense glycan shield. However, several of the recently identified PGT broadly neutralizing antibodies appear to interact directly with the HIV glycan coat. Crystal structures of Fabs PGT 127 and 128 with $Man_9$ at 1.65 and 1.29 Å resolution, respectively, and glycan binding data delineate a specific high mannose binding site. Fab PGT 128 complexed with a fully-glycosylated gp120 outer domain at 3.25 Å reveals that the antibody penetrates the glycan shield and recognizes two conserved glycans as well as a short β-strand segment of the gp120 V3 loop, accounting for its high binding

†To whom correspondence should be addressed: burton@scripps.edu (D.R.B.); wilson@scripps.edu (I.A.W.).
*These authors contributed equally to this work.

Supporting Online Material
www.sciencemag.org
Materials and Methods
figs. S1 to S13
tables S1 to S5
References 44-78 are SOM only

affinity and broad specificify. Furthermore, our data suggest that the high neutralization potency of PGT 127 and 128 IgGs may be mediated by cross-linking Env trimers on the viral surface.

Viruses have evolved a variety of mechanisms to escape antibody recognition, many of which involve features of the viral surface proteins, such as high variability, steric occlusion, and glycan coating. For HIV, the dense shield of glycans (1, 2) that decorate the viral Env protein was once believed to be refractory to antibody recognition, masking conserved functionally significant protein epitopes for which greater exposure would result in increased susceptibility to antibody neutralization. However, bnMAb 2G12 and several of the recently described PGT antibodies appear to bind directly to the HIV glycan coat. Although carbohydrate-protein interactions are typically weak (3), 2G12 recognizes terminal Manα1,2 Man moieties on oligomannose glycans using an unusual domain-exchanged antibody structure that creates a multivalent binding surface that enhances the affinity of the interaction through avidity effects (4). However, although 2G12 neutralizes clade B isolates broadly, it is less effective against other clades, particularly clade C viruses that have a somewhat different oligomannose glycan arrangement than clade B viruses. In contrast, we have recently isolated six bnMAbs (PGTs 125–128, 130–131) that bind specifically to the $Man_{8/9}$ glycans on gp120 and potently neutralize across clades (5). PGT 128, the broadest of these antibodies, neutralizes over 70% of globally circulating viruses and is, on average, an order of magnitude more potent than the recently described PG9, PG16, VRC01, and VRC-PG04 bnMAbs (6–8) and two orders of magnitude more potent than prototype bnMAbs described earlier (6, 9).

The neutralization potency exhibited by the PGT class of antibodies suggests that they may provide protection at relatively low serum concentrations. Hence, the epitopes recognized by these antibodies may be good vaccine targets if appropriate immunogens can be designed.

## Crystal structures of PGTs 127 and 128 bound to $Man_9$

To gain a structural understanding of the specificity for $Man_{8/9}$ glycans by PGTs 127 and 128, we first determined crystal structures of the antigen-binding fragments (Fabs) of PGTs 127 and 128 with a synthetic $Man_9$ glycan lacking the core N-acetylglucosamine (GlcNAc) moieties at 1.65 and 1.29Å resolution, respectively (table S1). The bound glycan is well ordered, except for the terminal mannose residue of the D2 arm (Fig. 1, fig. S1, and fig. S2A). The 127/$Man_9$ and 128/$Man_9$ structures show a similar conformation for the glycan (fig. S1), demonstrating a conserved mode of recognition by these clonally related antibodies.

Analysis of these crystal structures reveals the origin of their specificity for $Man_{8/9}$ glycans. The terminal mannose residues of both the D1 and D3 arms, which are only present on $Man_{8/9}$ glycans (Fig. 1B and fig. S2A), are heavily contacted, forming 11 of the 16 total hydrogen bonding interactions with the antibody (table S2). This specificity for glycans is consistent with glycan array data showing binding of PGT 127/8 to $Man_8$ and $Man_9$, but not to monoglucosylated $Man_9$ N-glycans (fig. S3A), and with glycosidase inhibitor specificity profiling (fig. S3B). The D3 arm of $Man_{8/9}$ is bound by CDR L3 residues Asn94, Trp95, and Asp95a (Fig. 1C and table S2). Several ordered water molecules are present in the glycan–antibody interface and also bridge the mannose residues (Fig. 1C), as previously noted as key features of other antibody-carbohydrate interfaces (10). In addition, two hydrogen bonds are observed between mannose residues that reside on different arms. The individual dihedrals of the glycan are in stable, low energy conformations (fig. S2), which are consistent with a high affinity interaction. PGTs 125–128 contain a 6-residue insertion in CDR H2 (5), which was likely introduced somatically during affinity maturation (11). This insertion mediates an outward displacement of the C″ β-strand of $V_H$ (fig. S4) and promotes

contact with the $Man_9$ D1 arm (Fig. 1 and table S2). Deletion of the insert resulted in diminished gp120 binding and neutralization potency for PGTs 127 and 128 (Fig. 3C). However, a reciprocal swap of the PGT 127 and 128 insert residues did not result in a complete interchange of their binding to gp120 or their neutralization profiles (Fig. 3C and fig. S5), indicating that the insert does not solely account for their differences in breadth and potency (12–13). The high affinity for $Man_9$ is explained by its extensive buried surface area (394 $Å^2$ by PGT 128 and 352 $Å^2$ by PGT 127) (table S2) in a binding mode that differs from other carbohydrate-binding antibodies or lectins and notably from 2G12, which only contacts the terminal Manα1,2 Man moieties of $Man_9$, particularly at the tip of the D1 arm (4).

## Crystal structure of PGT 128 bound to a glycosylated gp120 outer domain

To structurally define the glycan epitope recognized by PGT 128 in the context of gp120, we co-crystallized Fab PGT 128 with a glycosylated gp120 outer domain construct containing a truncated V3 loop (engineered outer domain mini-V3; eODmV3 (14)) (fig. S6). PGT 128 binds to eODmV3 with an apparent affinity of 46 nM, which is ~8-fold less than its interaction with HIV-$1_{JR-FL}$ gp120 core with a full-length V3 (fig. S7). Importantly, the V3 loop truncation did not affect PGT 128 binding (fig. S7). The purified complex was homogenous as assessed by SEC-MALS (fig. S8) and the crystal structure was solved by molecular replacement and refined at 3.25 Å resolution to an $R_{cryst}$ of 0.21 and $R_{free}$ of 0.26 (table S1).

The crystal structure unexpectedly revealed that PGT 128 engages two different glycans, as well as the C-terminal end of the V3 loop, within the binding site. The primary glycan-binding site is occupied by the high-mannose glycan attached to N332 ($Man_{8/9}GlcNAc_2$), while a secondary glycan-binding site is occupied by electron density associated with N301 (Fig. 2). The secondary glycan-binding site is focused on the core pentasaccharide attached to N301, as only the $Man_5GlcNAc_2$ portion of the glycan is visible in the density map (Fig. 2B). The two GlcNAc residues bind atop the CDR H1–H2 disulfide in a favorable hydrophobic interaction; hydrogen bonds are formed between the backbone amide and carbonyl of Ala52c and the N-acetyl and O3 hydroxyl of the first Asn-linked GlcNAc. FR3 and CDR H1 residues form the contact site for the mannose sugars (Fig. 2B and table S4).

The CDR H3 apex contacts the V3 loop on the gp120 outer domain. The C-terminal residues of V3, Ile323-Arg327, are bound in a groove between CDRs H2 and H3. Leu100-Asp100d in CDR H3 adopt a β-strand conformation that is primed for β-sheet type interactions with the gp120 V3 loop (15).

To assess the importance of the individual glycan binding sites for epitope recognition, we tested a series of antibody variants containing single amino-acid substitutions in each subsite. Mutations in the primary glycan binding site (N332) compromised neutralization, gp120 binding, and binding to $Man_{8/9}$ on the glycan array (Fig. 3A and table S3). Although numerous interactions are made with the glycan, including a total of 17 hydrogen bonds, disruption of the bidentate interaction between Man D3 and CDR L3 Asp95a resulted in a loss of gp120 and glycan binding and neutralizing activity (Fig. 3A). Mutation of residues involved in the secondary site (N301), particularly the H1–H2 disulfide, also resulted in a loss of gp120 binding and virus neutralization (Fig. 3B and table S3). Nevertheless, the affinity of this secondary site (N301) was too low to detect directly by glycan array, as evidenced by lack of glycan binding capacity by a primary glycan-binding site loss-of-function variant ($V_L$ Asp95a->Ala). Also, mutation of FR3 and CDR H1 residues that interact with the mannoses in the secondary binding site generally had little to no effect on neutralization by PGT 128, suggesting that the interactions with the mannose sugars in the

secondary site are not as crucial as the GlcNAc interactions (table S3). Notwithstanding, the N301 glycan is required for high-affinity binding to gp120 and neutralization. The importance of the N332 and N301 glycans in forming the PGT 128 epitope was confirmed by alanine scanning mutagenesis where substitutions at positions 332 and 301 resulted in loss of neutralizing activity against most isolates tested (table S5). PGT 127 displayed a similar glycan reactivity profile as PGT 128 against most isolates, suggesting that the two antibodies share a similar conserved mode of epitope recognition.

Notably, the N301 and N332 glycans are 93% and 73% conserved among HIV isolates (fig. S9), respectively, which accounts for the ability of PGT 128 to neutralize 72% of circulating viruses. Interestingly, in the HIV-$1_{JR\text{-}CSF}$ strain, individual alanine mutations at positions 332 and 301 had little to no effect on neutralization by PGT 128 (5), but various combinations of double glycan substitutions, which included the nearby N295 as well as N332 and N301, completely abolished neutralizing activity (fig. S10). These results suggest that, for JR-CSF, the epitope may be more promiscuous and accommodate antibody binding to two out of three glycans. The PGT 128 requirement for two closely spaced N-linked glycans (table S5 and fig. S10) likely accounts for its lack of reactivity with self-glycoproteins displaying single $Man_{8/9}GlcNAc_2$ (fig. S11) and for resistance of HIV-2 and SIV viruses to neutralization (fig. S12). Specific interactions with V3 were more difficult to investigate, as the V3 contacts with PGT 128 CDR H3 are primarily mediated through backbone hydrogen bonding and van der Waals interactions that are tolerant of side-chain variation, as seen for the V3 crown-specific antibody 447-52D (16). Thus, three discontinuous sites on the gp120 outer domain (449 $Å^2$ from N332, 328 $Å^2$ from N301, and 305 $Å^2$ from V3) combine to form 1081 $Å^2$ of buried surface area (table S4), which is similar in overall size to other anti-HIV bnMAbs VRC01 and VRC-PG04 that bury 1229 $Å^2$ and 1080 $Å^2$ on the CD4 binding site of core gp120, respectively (8, 17).

## The PGT 128 epitope is accessible on the HIV trimer

To gain a structural understanding of the epitope recognized by PGT 128 in the context of the HIV trimer, we generated a negative stain reconstruction of a soluble, partially deglycosylated 664G trimer in complex with PGT 128 Fab. This engineered Env trimer incorporates stabilizing mutations that allow it to maintain integrity upon deglycosylation (18–23). Three Fabs bind to the trimer with no close contacts to neighboring gp120 protomers, indicating that the outer domain epitope is accessible and exposed (Fig. 4A and fig. S13). Fitting of the crystal structure of the PGT 128/eODmV3 complex into the reconstruction also revealed that the V3 base (Fig. 4B and fig. S13D) is surface exposed, but below and adjacent to the density corresponding to the V1/V2 loops. No large-scale conformational changes in the trimer appear to take place upon Fab binding. Thus, the elements that form the PGT 128 epitope are almost directly opposite the CD4bs on gp120 and appear to be accessible and not subject to steric occlusion in the trimer.

## Mechanism of exceptional neutralization potency by PGTs 127 and 128

Since a strong correlation has been described in other systems between antibody apparent binding affinity for native Env trimers expressed on the cell surface and neutralization potency (24–27), we first compared the neutralization potency of PGTs 127 and 128 to their binding affinity for cell-surface expressed HIV-$1_{JR\text{-}FL}$ Env trimers (28–29). Interestingly, the neutralization $IC_{50}$ values of PGT 127 and 128 IgGs against HIV-$1_{JR\text{-}FL}$ were ~17- and 31- fold lower (i.e. more potent) than their cell-surface trimer-binding $EC_{50}$ values (Fig. 5), whereas the neutralization potency of Fabs PGT 127 and 128 correlated strongly with their binding affinity for cell surface HIV-$1_{JR\text{-}FL}$ Env trimers (Fig. 5). Furthermore, although PGT 127 and 128 IgGs bound with similar apparent affinity to cell surface Env trimers as

their Fab counterparts, they neutralized approximately 81- and 70-fold more potently, respectively, than their corresponding Fab fragments (Fig. 5). Similar results were also obtained with HIV-$1_{YU2}$ (fig. S14). Collectively, these results suggest that PGT 127 and 128 IgGs may cross-link spikes on the surface of the virus giving an increase in affinity through avidity effects, but not on the surface of Env expressing cells. The comparable binding affinity of PGT 127 and 128 IgGs and Fabs for cell-surface Env is consistent with IgG cross-linking of trimers on the viral surface occurring between spikes rather than within a single spike. In addition, intra-spike cross-linking by PGT 128 IgG appears unlikely based on the inter-Fab distances observed for PGT 128 Fab-trimer complexes by electron microscopy (Fig. 4). Considering the scarcity of native Env trimers on the viral surface (30), a possible explanation for this observation is that two or more viral spikes are clustered to form an infectious unit, as proposed previously (31). In this scenario, neutralization measures binding to infectious Env units, but not to single spikes. This interpretation also requires few infectious units on transfected cells compared to single spikes and that the single spikes are not in close enough proximity for cross-linking to occur. Notably, previous studies have reported that avidity generally plays a limited role in antibody neutralization of HIV, as suggested by the relatively modest increases in neutralization potencies of IgGs as compared to their Fab counterparts (32, 33). However, in contrast to other broadly neutralizing epitopes on HIV Env, the epitopes recognized by PGTs 127 and 128 appear to be highly accessible (Fig. 4), which may promote inter-spike cross-linking.

Previous studies in various virus systems, including murine leukemia virus (MLV), dengue virus (DENV), West Nile virus (WNV), poliovirus, and HIV, have shown that viral infectivity decays exponentially with time (34–36). Furthermore, certain NAbs have been shown to accelerate the decay of viral infectivity (37, 38). For example, recent studies have demonstrated the half-life of WNV and DENV decreases in the presence of virus-specific antibodies (37). To determine whether PGTs 127 and 128 impact the rate of viral infectivity decay, we measured the half-life of HIV-$1_{JR\text{-}FL}$ in the presence and absence of PGT 127 and 128 IgGs and Fabs. Interestingly, at antibody concentrations corresponding to 90% neutralization, PGTs 127 and 128 IgGs reduced the half-life of HIV-$1_{JR\text{-}FL}$ by approximately 9.7- and 11.2-fold, respectively, whereas the corresponding Fab fragments and 2G12 IgG had little to no effect on viral infectivity decay (Fig. 6A–B). Notably, no evidence for antibody-induced gp120 shedding was observed (fig. S15). Collectively, these data suggest that inter-spike cross-linking by PGT 127 and 128 IgGs may accelerate the inactivation of HIV-$1_{JR\text{-}FL}$ Env spikes, perhaps by inducing conformational changes that perturb trimer functionality (39), resulting in enhanced neutralization potency.

Studies of protein-carbohydrate interactions have established various principles of molecular recognition. For example, because glycan-protein interactions are weak due to unfavorable entropy contributions associated with glycan binding, multivalency is crucial to enhance binding affinity. Here, we provide an example of multivalency achieved through the combination of glycan and protein; the three sub-sites for N332, N301, and the C-terminal V3 stem are essentially independent, but combine to mediate high-affinity recognition of a glycan-based epitope on HIV Env. Considering the highly exposed nature of this epitope and the high conservation of its two glycan and V3 loop backbone components, coupled with recent studies demonstrating that broad and potent serum neutralizing activity is frequently mediated by antibodies that target N332A-sensitive epitopes (5, 40–43), it appears that this antigenic region may serve as an attractive vaccine target if appropriate immunogens can be designed.

## Supplementary Material

Refer to Web version on PubMed Central for supplementary material.

## Acknowledgments

We thank Y. Hua, K. Le, and V. Thaney for technical assistance, D. Ekiert for help with initial cloning of PGTs 125 and 126, X. Dai and X. Zhu for help with x-ray data collection and analysis, C. Corbaci and C. Williams for help with figure preparation, B. Walker for helpful comments on the manuscript, and members of The Glycosciences Laboratory for their collaboration in the establishment of the neoglycolipid-based microarray system. This work was supported by the International AIDS Vaccine Initiative Neutralizing Antibody Center, NIH AI84817 (I.A.W.), NIAID AI33292 (D.R.B.), NIH/NRSA fellowship AI74372 (R.P.), Canadian Institutes of Health Research (CIHR) fellowship, FRN HFE-224662 (J.-P.J.), HIVRAD AI082362 (W.C.O., J.P.M., and I.A.W.), UK Research Councils' Basic Technology Initiative 'Glycoarrays' (GRS/79268), EPSRC Translational Grant (EP/G037604/1) and NCI Alliance of Glycobiologists for Detection of Cancer and Cancer Risk (U01 CA128416), and the Ragon Institute. The 3D reconstructions were conducted at the National Resource for Automated Molecular Microscopy (NRAMM), which is supported by the National Institutes of Health through the National Center for Research Resources' P41 program (RR017573). Portions of this research were carried out at the Stanford Synchrotron Radiation Lightsource, a Directorate of SLAC National Accelerator Laboratory and an Office of Science User Facility operated for the U.S. Department of Energy Office of Science by Stanford University. The SSRL Structural Molecular Biology Program is supported by the DOE Office of Biological and Environmental Research, and by the National Institutes of Health, National Center for Research Resources, Biomedical Technology Program (P41RR001209), and the National Institute of General Medical Sciences. Use of the Advanced Photon Source was supported by the U.S. Department of Energy, Basic Energy Sciences, Office of Science, under contract No. DE-AC02-06CH11357. GM/CA CAT has been funded in whole or in part with Federal funds from the National Cancer Institute (Y1-CO-1020) and the National Institute of General Medical Sciences (Y1-GM-1104). Coordinates and structure factors for the Fab PGT 128/Man9, Fab PGT 127/Man9, and Fab PGT 128/eODmV3 structures have been deposited with the PDB under accession codes 3TV3, 3TWC, and 3TYG. The Fab PGT 128/d664G trimer EM reconstruction density has been deposited with the EMDB under accession code EMD-1970. This is manuscript 21407-MB from The Scripps Research Institute.

## References and Notes

1. Kwong PD, et al. Structure of an HIV gp120 envelope glycoprotein in complex with the CD4 receptor and a neutralizing human antibody. Nature. 1998; 393:648–659. [PubMed: 9641677]
2. Wyatt R, Sodroski J. The HIV-1 envelope glycoproteins: fusogens, antigens, and immunogens. Science. 1998; 280:1884–1888. [PubMed: 9632381]
3. Toone EJ. Structure and energetics of protein-carbohydrate complexes. Curr Opin Struct Biol. 1994; 4:719–728.
4. Calarese DA, et al. Antibody domain exchange is an immunological solution to carbohydrate cluster recognition. Science. 2003; 300:2065–2071. [PubMed: 12829775]
5. Walker LM, et al. Broad neutralization coverage of HIV by multiple highly potent antibodies. Nature. 2011; 477:466–470. [PubMed: 21849977]
6. Walker LM, et al. Broad and potent neutralizing antibodies from an African donor reveal a new HIV-1 vaccine target. Science. 2009; 326:285–289. [PubMed: 19729618]
7. Wu X, et al. Rational design of envelope identifies broadly neutralizing human monoclonal antibodies to HIV-1. Science. 2010; 329:856–861. [PubMed: 20616233]
8. Wu X, et al. Focused evolution of HIV-1 neutralizing antibodies revealed by structures and deep sequencing. Science. 2011; 333:1593–1602. [PubMed: 21835983]
9. Binley JM, et al. Comprehensive cross-clade neutralization analysis of a panel of anti-human immunodeficiency virus type 1 monoclonal antibodies. J Virol. 2004; 78:13232–13252. [PubMed: 15542675]
10. Wilson IA, Stanfield RL. A Trojan horse with a sweet tooth. Nat Struct Biol. 1995; 2:433–436. [PubMed: 7664102]
11. Wilson PC, et al. Somatic hypermutation introduces insertions and deletions into immunoglobulin V genes. J Exp Med. 1998; 187:59–70. [PubMed: 9419211]
12. Krause JC, et al. An insertion mutation that distorts antibody binding site architecture enhances function of a human antibody. MBio. 2011; 2:e00345–00310. [PubMed: 21304166]
13. Notably, it has been shown that a three-amino-acid insertion in the heavy-chain CDR H2 of the influenza virus-specific MAb 2D1 rearranges the antibody-combining site and enhances neutralization potency (12), demonstrating that somatically introduced amino-acid insertions may be a conserved molecular mechanism for increasing antibody potency against viral pathogens.

14. The eODmV3 was expressed in GnTI −/− deficient HEK 293S cells to mimic the oligomannose-type glycosylation of that domain within intact gp120.
15. Three canonical strand-pairing H-bonds are formed as well as an H-bond between V3 Asp325 and the backbone amide of $Asp^{H100d}$ (Fig. 2C). Ile323 also interacts with the CDR H1-H2 disulfide and with $Leu^{H100}$ in CDR H3, and Arg327 is located in close proximity to $Asp^{H100d}$. $Tyr^{H100b}$ makes aromatic interaction with the Gly324-Asp325 peptide bond. Also, similar to many other anti-HIV bnMAbs, the PGT 128 CDR H3 loop is relatively long (19 amino acids), although not the longest seen to date for human Abs (31–32 residues for the PGT 140 series (5))
16. Stanfield RL, Gorny MK, Williams C, Zolla-Pazner S, Wilson IA. Structural rationale for the broad neutralization of HIV-1 by human monoclonal antibody 447-52D. Structure. 2004; 12:193–204. [PubMed: 14962380]
17. Zhou T, et al. Structural basis for broad and potent neutralization of HIV-1 by antibody VRC01. Science. 2010; 329:811–817. [PubMed: 20616231]
18. Beddows S, et al. Construction and characterization of soluble, cleaved, and stabilized trimeric Env proteins based on HIV type 1 Env subtype A. AIDS Res Hum Retroviruses. 2006; 22:569–579. [PubMed: 16796532]
19. Binley JM, et al. A recombinant human immunodeficiency virus type 1 envelope glycoprotein complex stabilized by an intermolecular disulfide bond between the gp120 and gp41 subunits is an antigenic mimic of the trimeric virion-associated structure. J Virol. 2000; 74:627–643. [PubMed: 10623724]
20. Binley JM, et al. Enhancing the proteolytic maturation of human immunodeficiency virus type 1 envelope glycoproteins. J Virol. 2002; 76:2606–2616. [PubMed: 11861826]
21. Sanders RW, et al. Stabilization of the soluble, cleaved, trimeric form of the envelope glycoprotein complex of human immunodeficiency virus type 1. J Virol. 2002; 76:8875–8889. [PubMed: 12163607]
22. Harris A, et al. Trimeric HIV-1 glycoprotein gp140 immunogens and native HIV-1 envelope glycoproteins display the same closed and open quaternary molecular architectures. Proc Natl Acad Sci USA. 2011; 108:11440–11445. [PubMed: 21709254]
23. The HIV-1 664G trimer is based on the clade A strain KNH1144 and incorporates stabilizing mutations A501C, T605C, and I559P. We have previously shown that trimers incorporating these stabilizing mutations are competent to undergo CD4-induced conformational changes akin to those observed in the native trimer (22).
24. Parren PW, Burton DR. The antiviral activity of antibodies in vitro and in vivo. Adv Immunol. 2001; 77:195–262. [PubMed: 11293117]
25. Parren PW, et al. Neutralization of human immunodeficiency virus type 1 by antibody to gp120 is determined primarily by occupancy of sites on the virion irrespective of epitope specificity. J Virol. 1998; 72:3512–3519. [PubMed: 9557629]
26. Roben P, et al. Recognition properties of a panel of human recombinant Fab fragments to the CD4 binding site of gp120 that show differing abilities to neutralize human immunodeficiency virus type 1. J Virol. 1994; 68:4821–4828. [PubMed: 7518527]
27. Sattentau QJ, Moore JP. Human immunodeficiency virus type 1 neutralization is determined by epitope exposure on the gp120 oligomer. J Exp Med. 1995; 182:185–196. [PubMed: 7540648]
28. Pancera M, Wyatt R. Selective recognition of oligomeric HIV-1 primary isolate envelope glycoproteins by potently neutralizing ligands requires efficient precursor cleavage. Virology. 2005; 332:145–156. [PubMed: 15661147]
29. $HIV\text{-}1_{JR\text{-}FL}$ is the only HIV isolate that has been shown to express a high proportion of fully cleaved Env trimers on the surface of transfected cells and was, therefore, selected for binding studies.
30. Liu J, Bartesaghi A, Borgnia MJ, Sapiro G, Subramaniam S. Molecular architecture of native HIV-1 gp120 trimers. Nature. 2008; 455:109–113. [PubMed: 18668044]
31. Klasse PJ. Modeling how many envelope glycoprotein trimers per virion participate in human immunodeficiency virus infectivity and its neutralization by antibody. Virology. 2007; 369:245–262. [PubMed: 17825343]

32. Klein JS, Bjorkman PJ. Few and far between: how HIV may be evading antibody avidity. PLoS Pathogens. 2010; 6:e1000908. [PubMed: 20523901]
33. Klein JS, et al. Examination of the contributions of size and avidity to the neutralization mechanisms of the anti-HIV antibodies b12 and 4E10. Proc Natl Acad Sci USA. 2009; 106:7385–7390. [PubMed: 19372381]
34. Ansarah-Sobrinho C, Nelson S, Jost CA, Whitehead SS, Pierson TC. Temperature-dependent production of pseudoinfectious dengue reporter virus particles by complementation. Virology. 2008; 381:67–74. [PubMed: 18801552]
35. Layne SP, et al. Factors underlying spontaneous inactivation and susceptibility to neutralization of human immunodeficiency virus. Virology. 1992; 189:695–714. [PubMed: 1386485]
36. Le Doux JM, Davis HE, Morgan JR, Yarmush ML. Kinetics of retrovirus production and decay. Biotechnol Bioeng. 1999; 63:654–662. [PubMed: 10397822]
37. Dowd KA, Jost CA, Durbin AP, Whitehead SS, Pierson TC. A dynamic landscape for antibody binding modulates antibody-mediated neutralization of west nile virus. PLoS Pathogens. 2011; 7:e1002111. [PubMed: 21738473]
38. Ruprecht CR, et al. MPER-specific antibodies induce gp120 shedding and irreversibly neutralize HIV-1. J Exp Med. 2011; 208:439–454. [PubMed: 21357743]
39. Haim H, et al. Soluble CD4 and CD4-mimetic compounds inhibit HIV-1 infection by induction of a short-lived activated state. PLoS Pathogens. 2009; 5:e1000360. [PubMed: 19343205]
40. Gray ES, et al. The neutralization breadth of HIV-1 develops incrementally over four years and is associated with CD4+ T cell decline and high viral load during acute infection. J Virol. 2011; 85:4828–4840. [PubMed: 21389135]
41. Walker LM, et al. A limited number of antibody specificities mediate broad and potent serum neutralization in selected HIV-1 infected individuals. PLoS Pathogens. 2010; 6:e1001028. [PubMed: 20700449]
42. Tang H, et al. Epitopes immediately below the base of the V3 loop of gp120 as targets for the initial autologous neutralizing antibody response in two HIV-1 subtype B-infected individuals. J Virol. 2011; 85:9286–9299. [PubMed: 21734041]
43. Nandi A, et al. Epitopes for broad and potent neutralizing antibody responses during chronic infection with human immunodeficiency virus type 1. Virology. 2010; 392:339–348. [PubMed: 19922969]
44. Pejchal R, et al. Structure and function of broadly reactive antibody PG16 reveal an H3 subdomain that mediates potent neutralization of HIV-1. Proc Natl Acad Sci USA. 2010; 107:11483–11488. [PubMed: 20534513]
45. Reeves PJ, Callewaert N, Contreras R, Khorana HG. Structure and function in rhodopsin: high-level expression of rhodopsin with restricted and homogeneous N-glycosylation by a tetracycline-inducible N-acetylglucosaminyltransferase I-negative HEK293S stable mammalian cell line. Proc Natl Acad Sci USA. 2002; 99:13419–13424. [PubMed: 12370423]
46. Folta-Stogniew E. Oligomeric states of proteins determined by size-exclusion chromatography coupled with light scattering, absorbance, and refractive index detectors. Methods Mol Biol. 2006; 328:97–112. [PubMed: 16785643]
47. Lee HK, et al. Reactivity-based one-pot synthesis of oligomannoses: defining antigens recognized by 2G12, a broadly neutralizing anti-HIV-1 antibody. Angew Chem Int Ed Engl. 2004; 43:1000–1003. [PubMed: 14966891]
48. McCoy AJ, et al. Phaser crystallographic software. J Appl Crystallogr. 2007; 40:658–674. [PubMed: 19461840]
49. The CCP4 suite: programs for protein crystallography. Acta Crystallogr D Biol Crystallogr. 1994; 50:760–763. [PubMed: 15299374]
50. Duquerroy S, et al. Crystal structure of a human autoimmune complex between IgM rheumatoid factor RF61 and IgG1 Fc reveals a novel epitope and evidence for affinity maturation. J Mol Biol. 2007; 368:1321–1331. [PubMed: 17395205]
51. Adams PD, et al. PHENIX: building new software for automated crystallographic structure determination. Acta Crystallogr D Biol Crystallogr. 2002; 58:1948–1954. [PubMed: 12393927]

52. Emsley P, Cowtan K. Coot: model-building tools for molecular graphics. Acta Crystallogr D Biol Crystallogr. 2004; 60:2126–2132. [PubMed: 15572765]
53. Blanc E, et al. Refinement of severely incomplete structures with maximum likelihood in BUSTER-TNT. Acta Crystallogr D Biol Crystallogr. 2004; 60:2210–2221. [PubMed: 15572774]
54. Strong M, et al. Toward the structural genomics of complexes: crystal structure of a PE/PPE protein complex from *Mycobacterium tuberculosis*. Proc Natl Acad Sci USA. 2006; 103:8060–8065. [PubMed: 16690741]
55. Otwinowski Z, Minor W. Processing of x-ray diffraction data collected in oscillation mode. Methods Enzymol. 1997; 276:307–326.
56. DeLaBarre B, Brunger AT. Considerations for the refinement of low-resolution crystal structures. Acta Crystallogr D Biol Crystallogr. 2006; 62:923–932. [PubMed: 16855310]
57. Lander GC, et al. Appion: an integrated, database-driven pipeline to facilitate EM image processing. J Struct Biol. 2009; 166:95–102. [PubMed: 19263523]
58. Voss NR, Yoshioka CK, Radermacher M, Potter CS, Carragher B. DoG Picker and TiltPicker: software tools to facilitate particle selection in single particle electron microscopy. J Struct Biol. 2009; 166:205–213. [PubMed: 19374019]
59. Mindell JA, Grigorieff N. Accurate determination of local defocus and specimen tilt in electron microscopy. J Struct Biol. 2003; 142:334–347. [PubMed: 12781660]
60. Hohn M, et al. SPARX, a new environment for Cryo-EM image processing. J Struct Biol. 2007; 157:47–55. [PubMed: 16931051]
61. Tang G, et al. EMAN2: an extensible image processing suite for electron microscopy. J Struct Biol. 2007; 157:38–46. [PubMed: 16859925]
62. Ludtke SJ, Baldwin PR, Chiu W. EMAN: semiautomated software for high-resolution single-particle reconstructions. J Struct Biol. 1999; 128:82–97. [PubMed: 10600563]
63. Li M, et al. Human immunodeficiency virus type 1 env clones from acute and early subtype B infections for standardized assessments of vaccine-elicited neutralizing antibodies. J Virol. 2005; 79:10108–10125. [PubMed: 16051804]
64. Montefiori DC. Evaluating neutralizing antibodies against HIV, SIV, and SHIV in luciferase reporter gene assays. Curr Protoc Immunol. 2005; Chapter 12(Unit 12):11. [PubMed: 18432938]
65. Doores KJ, et al. Variable loop glycan dependency of the broad and potent HIV- 1-neutralizing antibodies PG9 and PG16. J Virol. 2010; 84:10510–10521. [PubMed: 20686044]
66. Matsuo I, Ito Y. Synthesis of an octamannosyled glycan chain, the key oligosaccharide structure in ER-associated degradation. Carbohydr Res. 2003; 338:2163–2168. [PubMed: 14553976]
67. Totani K, Matsuo I, Ihara Y, Ito Y. High-mannose-type glycan modifications of dihydrofolate reductase using glycan-methotrexate conjugates. Bioorg Med Chem. 2006; 14:5220–5229. [PubMed: 16647263]
68. Wang SK, et al. Targeting the carbohydrates on HIV-1: Interaction of oligomannose dendrons with human monoclonal antibody 2G12 and DC-SIGN. Proc Natl Acad Sci USA. 2008; 105:3690–3695. [PubMed: 18310320]
69. Blixt O, et al. Printed covalent glycan array for ligand profiling of diverse glycan binding proteins. Proc Natl Acad Sci. 2004; 101:17033–17038. [PubMed: 15563589]
70. Chai W, Stoll MS, Galustian C, Lawson AM, Feizi T. Neoglycolipid technology: deciphering information content of glycome. Methods Enzymol. 2003; 362:160–195. [PubMed: 12968363]
71. Liu Y, et al. Neoglycolipid probes prepared via oxime ligation for microarray analysis of oligosaccharide-protein interactions. Chem Biol. 2007; 14:847–859. [PubMed: 17656321]
72. Palma AS, et al. Ligands for the beta-glucan receptor, Dectin-1, assigned using “designer” microarrays of oligosaccharide probes (neoglycolipids) generated from glucan polysaccharides. J Biol Chem. 2006; 281:5771–5779. [PubMed: 16371356]
73. Dunlop DC, et al. Polysaccharide mimicry of the epitope of the broadly neutralizing anti-HIV antibody, 2G12, induces enhanced antibody responses to self oligomannose glycans. Glycobiology. 2010; 20:812–823. [PubMed: 20181792]

74. Petrescu AJ, Petrescu SM, Dwek RA, Wormald MR. A statistical analysis of N- and O-glycan linkage conformations from crystallographic data. Glycobiology. 1999; 9:343–352. [PubMed: 10089208]

75. Lutteke T, Frank M, von der Lieth CW. Carbohydrate Structure Suite (CSS): analysis of carbohydrate 3D structures derived from the PDB. Nucleic Acids Res. 2005; 33:D242–246. [PubMed: 15608187]

76. Zhou T, et al. Structural definition of a conserved neutralization epitope on HIV-1 gp120. Nature. 2007; 445:732–737. [PubMed: 17301785]

77. Sheriff S, Hendrickson WA, Smith JL. Structure of myohemerythrin in the azidomet state at 1.7/1.3 Å resolution. J Mol Biol. 1987; 197:273–296. [PubMed: 3681996]

78. Connolly ML. The molecular surface package. J Mol Graph. 1993; 11:139–141. [PubMed: 8347567]

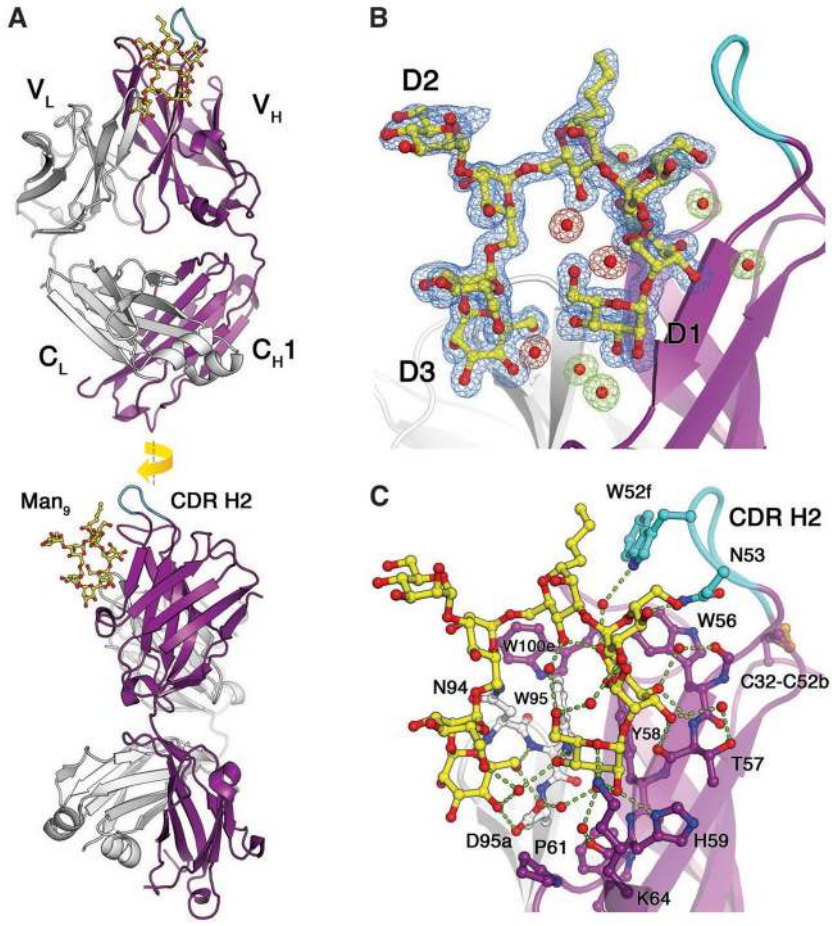


**Fig. 1.**

Unique binding mode of $Man_9$ by antibody PGT 128 revealed by the high-resolution crystal structure of the complex. **(A)** Front (top) and side (bottom) views of PGT 128 Fab with bound $Man_9$ glycan. The light and heavy chains are depicted as grey and magenta ribbons, respectively, and the glycan as yellow (carbons) and red (oxygen) ball-and sticks. **(B)** Close-up view of glycan binding site of PGT 128 showing electron density (2Fo-Fc) at 1.0 sigma for glycan and associated water molecules. Water molecules are shown as red spheres with the electron density colored red for waters that bridge mannose residues and green for waters in the glycan-antibody interface. **(C)** Detailed view of the interactions in the $Man_9$ glycan binding site at the interface of CDRs H2, H3, L3 and FR2. Tryptophan ($V_H$ W52f, W56, W100e and $V_L$ W95) and Asn/Asp ($V_H$ N53, $V_L$ N94, D95a) residues from the Fab are enriched in the interface and dominate the interactions with the glycan. The D1 arm is bound by residues in the 6-amino acid CDR H2 insert and $V_H$ FR2. The D3 arm is bound by residues within CDR L3. Hydrogen bonds are shown as green dashes.

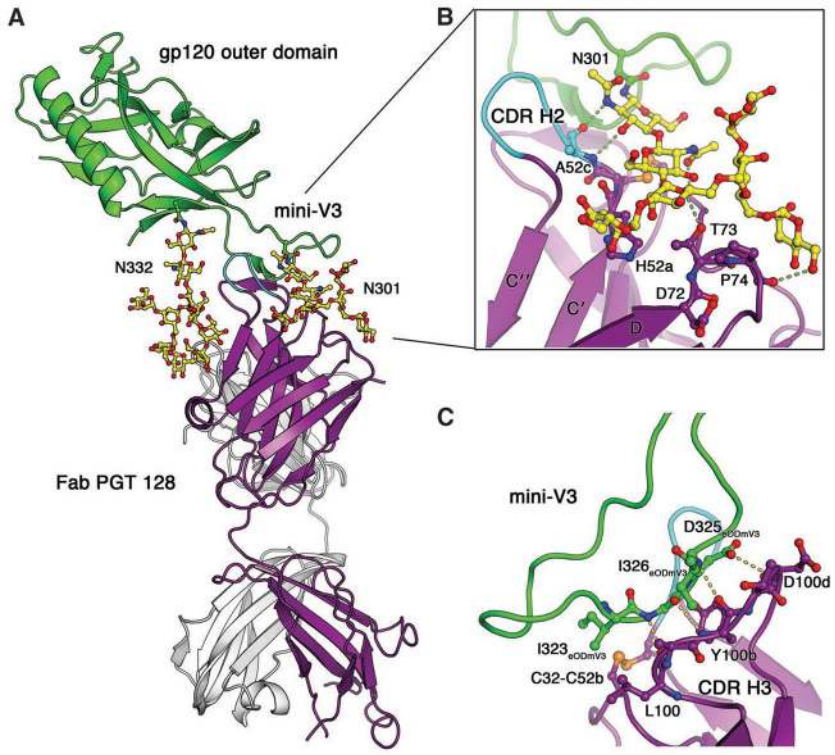


**Fig. 2.**

Crystal structure of PGT 128 Fab in complex with an engineered glycosylated gp120 outer domain (eODmV3). **(A)** Overall view of PGT 128/eODmV3. PGT 128 Fab heavy and light chains are depicted as in Fig. 1. The eODmV3 is shown in a green cartoon ribbon representation. Glycans are depicted in a ball-and-stick representation with carbons in yellow, oxygens in red and nitrogens in blue. PGT 128 binds the N332 glycan in the primary glycan binding site by interactions with the terminal mannose residues of the D1 and D3 arms. The mode of interaction and site of recognition is identical to that visualized in the high resolution $Man_9$ complex. The secondary glycan binding site recognizes the N301 glycan. **(B)** Close up view of the secondary glycan interaction site and contacts made with N301 glycan. The mannose residues of the N301 glycan splay out around FR3 residues $V_H$ D72, T73, P74, and K75. The terminal mannose resides are not ordered in the electron density. **(C)** Close up view of V3 interactions with CDR H3. The C-terminus of V3, residues D325-Q328, makes van der Waals and hydrogen bonding contacts to one side of an extended β-strand region of PGT 128 CDR H3, which includes L100-D100d. The V3 base is intercalated between the apex of the CDR H2 insert (Y52e and W52f) and CDR H3.

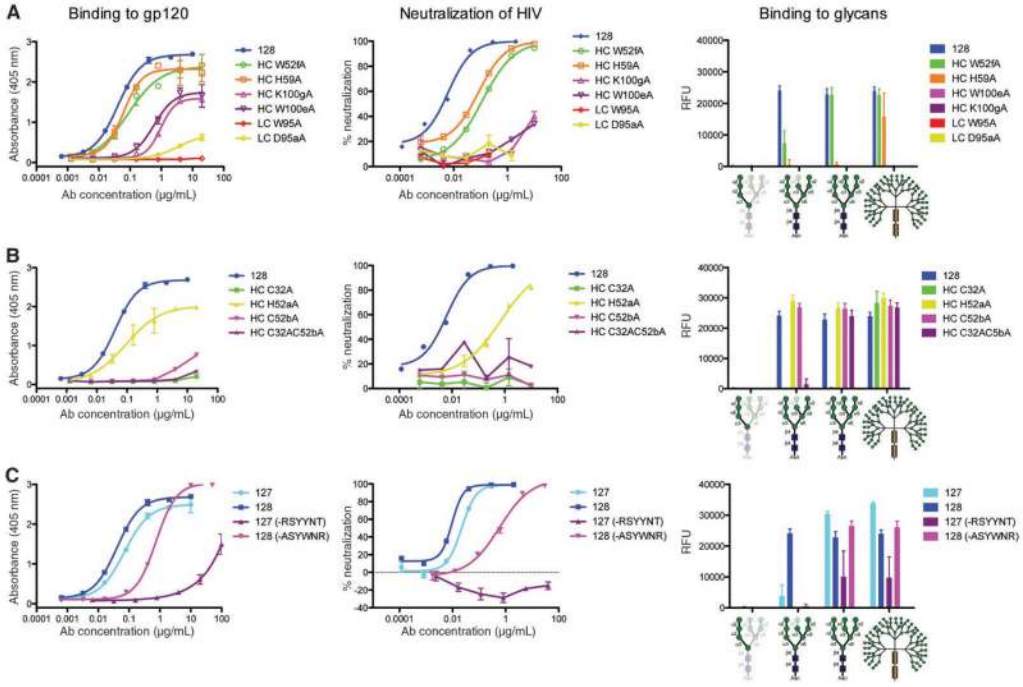


**Fig. 3.**

Effect of PGT 128 paratope mutations in the individual glycan subsites on neutralization of HIV-$1_{JR\text{-}FL}$ and glycan binding. Binding of PGT 128 mutants to gp120 was tested by ELISA (left panel) or to glycans on the high mannose glycan microarray (right panel). **(A)** Mutation of select residues in the primary glycan binding site ($Man_{8/9}$) that recognizes the N332 glycan. Residues (HC, heavy chain; LC, light chain) that disrupt the formation of the hydrophobic core of the binding site ($V_H$ K100gA, W100eA, and $V_L$ W95A) or disrupt hydrogen bonding to terminal mannose residues ($V_H$ H59A and $V_L$ D95aA) compromise neutralization (middle panel), as well as gp120 and glycan binding. **(B)** Mutation of select residues interacting with the secondary glycan binding site that recognizes the N301 glycan. Mutation of $V_H$ H52aA results in a decrease in gp120 binding and neutralization, while disruption of the CDR H1–H2 disulfide ($V_H$ C32A, C52bA, or double mutant) greatly compromises both gp120 binding and neutralization. There is much less effect on the glycan array which primarily reflects binding to the primary glycan binding site. A complete list of paratope mapping, as well as the effect on gp120 binding, is provided in Table S3. **(C)** Contribution of the 6-residue CDR H2 insert to neutralization and glycan binding. PGT 128 retains the ability to bind $Man_{8/9}$ and neutralize to a lesser extent on deletion of the insert, whereas PGT 127 no longer neutralizes, although still has some ability to bind $Man_{8/9}$. Swapping of the insert between 127 and 128 allows 128 to retain some binding and neutralization, but substantially reduces binding and abrogates neutralization when the PGT 128 H2 insert is transplanted onto PGT 127.

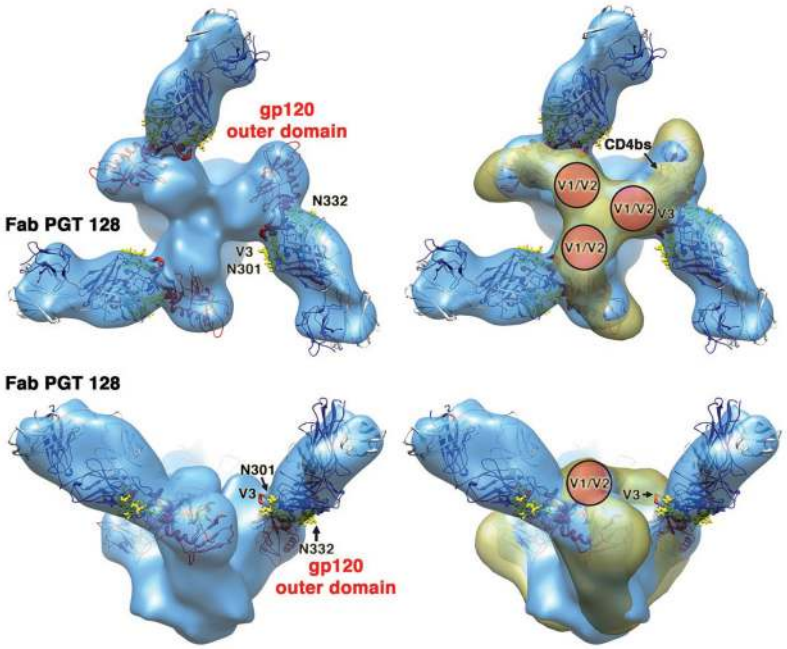


**Fig. 4.**

Negative stain reconstruction of partially-deglycosylated soluble 664G Env trimer in complex with PGT 128 Fab. Soluble (664G) Env trimer was complexed with Fab PGT 128 and treated with Endo H to remove non-protected glycans. **(A)** Coordinates of the 128/eODmV3 complex structure fitted into the reconstruction density (blue). Overhead (top) and side (bottom) views show the fit of the crystal structure to the EM density (see SOM). Fab 128, depicted as blue (heavy) and white (light), and eODmV3 (red) are depicted in schematic backbone representation with glycans shown as yellow sticks. **(B)** Reconstruction density overlayed with cryo-electron tomographic reconstruction of native, unliganded trimer (yellow) (30). The putative location of V1/V2 is indicated. V3, N301, and N332 are exposed on the surface of the outer domain and slightly below the trimer apex, which corresponds to location of the V1/V2 loops. The PGT 128 epitope is located approximately on the opposite side of gp120 from the CD4bs (fig. S13C).

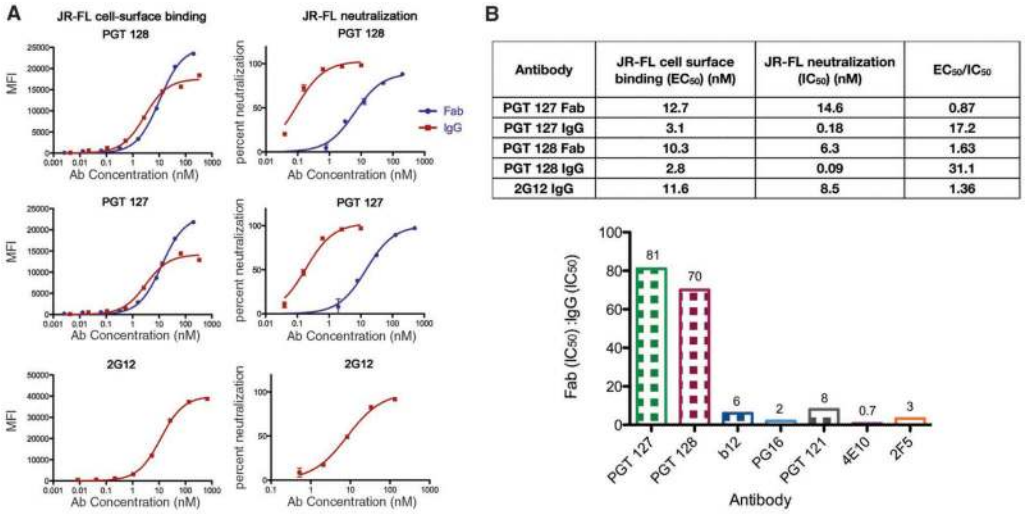


**Fig. 5.**

Cell-surface binding and neutralization properties of PGT 127 and PGT 128 IgGs and Fabs. **(A)** (left) Binding of PGT 127 and PGT 128 Fabs and IgGs to HIV-$1_{JR-FL}$ trimers expressed on the surface of transfected 293T cells as determined by flow cytometry. (right) Neutralizing activity of PGT 127 and PGT 128 IgGs and Fabs against HIV-$1_{JR-FL}$. 2G12 is included for comparison. Experiments were performed in duplicate and data are representative of at least two independent experiments. MFI, mean fluorescence intensity. **(B)** (top) Comparison of binding ($EC_{50}$) and neutralization ($IC_{50}$) for PGT 127 and PGT 128 Fabs and IgGs against HIV-$1_{JR-FL}$. 2G12 is included for comparison. (bottom) Bar graph representation of Fab ($IC_{50}$): IgG ($IC_{50}$) ratios for PGT 127, PGT 128, b12, PG16, PGT 121, 2F5, and 4E10. 2G12 is not included as its two Fabs form a domain-swapped dimer (4). Ratios were calculated as $IC_{50}$ of the Fab / $IC_{50}$ of IgG.

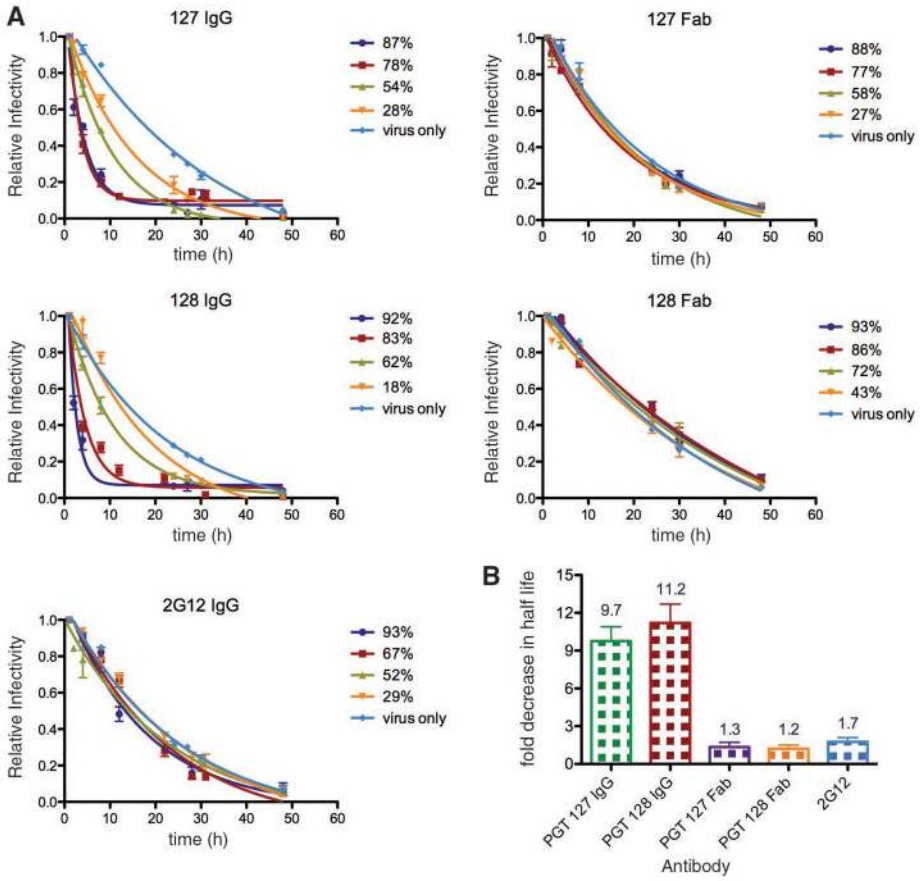


**Fig. 6.**

Impact of PGT 127 and PGT 128 on viral infectivity decay. **(A)** Viral infectivity decay of HIV-$1_{JR\text{-}FL}$ was measured in the presence of PGT 127 and PGT 128 IgGs and Fabs. 2G12 is included for comparison. Data were fitted to a single-phase exponential decay to obtain half-life. Individual experiments were performed in triplicate, and error bars represent the standard error of two independent experiments. **(B)** The reduction in the half-life of HIV-$1_{JR\text{-}FL}$ (expressed as an x-fold decrease) in the presence of antibodies at concentrations providing 90% neutralization, compared to the absence of antibody. Error bars represent the standard error of two independent experiments.